

This discussion paper is/has been under review for the journal Atmospheric Measurement Techniques (AMT). Please refer to the corresponding final paper in AMT if available.

# Cross-track Infrared Sounder (CrIS) satellite observations of tropospheric ammonia

M. W. Shephard<sup>1</sup> and K. E. Cady-Pereira<sup>2</sup>

<sup>1</sup>Environment Canada, Toronto, Ontario, Canada

<sup>2</sup>Atmospheric and Environmental Research, Inc., Lexington, Massachusetts, USA

Received: 23 September 2014 – Accepted: 20 October 2014 – Published: 19 November 2014

Correspondence to: M. W. Shephard (mark.shephard@ec.gc.ca)

Published by Copernicus Publications on behalf of the European Geosciences Union.

AMTD

7, 11379–11413, 2014

**CrIS satellite  
observations of NH<sub>3</sub>**

M. W. Shephard and  
K. E. Cady-Pereira

Title Page

Abstract

Introduction

Conclusions

References

Tables

Figures

◀

▶

◀

▶

Back

Close

Full Screen / Esc

Printer-friendly Version

Interactive Discussion



## Abstract

Observations of atmospheric ammonia are important in understanding and modeling the impact of ammonia on both human health and the natural environment. Presented is a detailed description of a robust retrieval algorithm that demonstrates the capabilities of utilizing Cross-track Infrared Sounder (CrIS) satellite observations to globally retrieve ammonia concentrations. Initial ammonia retrieval results using both simulated and real observations show that CrIS is: (i) sensitive to ammonia in the boundary layer, with peak vertical sensitivity typically around 800 hPa ( $\sim 2$  km), (ii) has a minimum detection limit of  $\sim 1$  ppbv (peak profile value), and (iii) the information content can vary significantly with peak values of  $\sim 1$  degrees-of-freedom for signal. Comparisons of the retrieval with simulated “true” profiles show there is small positive retrieval bias of 6 %, with the variability being from 4 % (25th quartile) to +26 % (75th quartile). Note these uncertainty estimates are considered as lower bound values as no potential systematic errors are included in the simulations. The CrIS NH<sub>3</sub> retrieval applied over the Central Valley in CA, USA demonstrates that CrIS can capture the general spatial variability of the boundary layer ammonia concentrations seen by the nearby Quantum Cascade-Laser (QCL) in-situ surface and the Tropospheric Emission Spectrometer (TES) satellite observations as part of the DISCOVER-AQ campaign. The CrIS and TES ammonia observations show quantitatively similar retrieved boundary layer values that are often within the uncertainty of the two observations. These initial results demonstrate the capabilities of the CrIS satellite to measure ammonia.

## 1 Introduction

Ammonia, along with ammonium nitrate and ammonium sulfate aerosols, is important for the nitrogen cycle that directly or indirectly impact air quality, water quality, and the climate. In the atmosphere ammonia is a toxin, and it combines with sulfates and nitric acid to form ammonium nitrate and ammonium sulfate, which constitute a substantial

AMTD

7, 11379–11413, 2014

## CrIS satellite observations of NH<sub>3</sub>

M. W. Shephard and  
K. E. Cady-Pereira

Title Page

Abstract

Introduction

Conclusions

References

Tables

Figures

◀

▶

◀

▶

Back

Close

Full Screen / Esc

Printer-friendly Version

Interactive Discussion



fraction of fine particulate matter ( $\text{PM}_{2.5}$ ) (e.g. Seinfeld and Pandis, 1988). These particles form smog and, in addition to being statistically associated with health impacts (e.g. bronchitis, asthma, cardiovascular disease, and premature deaths, Pope et al., 2000), also have climate impacts. In terms of climate change, ammonia's contribution to atmospheric aerosols has both a direct (reflection of solar radiation) and indirect (clouds) radiative forcing effect (e.g. Charlson et al., 1991). Furthermore, reactive nitrogen (Nr) (e.g. ammonia ( $\text{NH}_3$ ), ammonium ( $\text{NH}_4^+$ ), nitrogen oxide (NO)) has increased by a factor of three-to-five over the last century (Reay et al., 2008), and anthropogenic ammonia gas emissions (i.e. concentrated animal feeding operations (CAFO), fertilizers, biofuel) are one of the IPCC AR5 Representative Pathway Concentration (RPC) species predicted to increase in the future (Lamarque et al., 2010). Increasing atmospheric concentrations of ammonia have the potential to increase the global deposition of reactive nitrogen to nitrogen poor ecosystems, which in turn increases the efficiency of the land and ocean in removing human-induced carbon dioxide from the atmosphere, thus acting as a carbon sink ("carbon dioxide fertilization effect", Reay et al., 2008). Excess deposition in terrestrial ecosystems leads to soil acidification and loss of biodiversity (e.g. Carfara et al., 2004); and in coastal ecosystems causes, eutrophication, algal blooms, and loss of fish and shellfish (e.g. Paerl et al., 2002). In spite of the significant role ammonia plays in our environment and health, there is still limited knowledge of the magnitude and seasonal/spatial distribution of  $\text{NH}_3$  emission sources, especially on a global scale. Therefore, satellite observations of ammonia provide an unprecedented opportunity to gain a greater understanding of atmospheric ammonia concentrations and to constrain model emission, which are still poorly known, especially outside of North America and Europe.

Observations from the NASA Aura Tropospheric Emission Spectrometer (TES) (Beer et al., 2001) Fourier Transform Spectrometer (FTS) launched on 15 July 2004, and the Infrared Atmospheric Sounder Interferometer (IASI) (Clerbaux et al., 2009) FTS launched on MetOp-A (19 October 2006) and MetOp-B (17 September 2012), have demonstrated the value of lower tropospheric ammonia satellite measurements. For

**CrlS satellite observations of  $\text{NH}_3$** M. W. Shephard and  
K. E. Cady-Pereira[Title Page](#)[Abstract](#)[Introduction](#)[Conclusions](#)[References](#)[Tables](#)[Figures](#)[|◀](#)[▶|](#)[◀](#)[▶](#)[Back](#)[Close](#)[Full Screen / Esc](#)[Printer-friendly Version](#)[Interactive Discussion](#)

example, IASI and TES observations have shown spatial and seasonal distributions of ambient tropospheric ammonia concentrations globally (Clarisso et al., 2009; Shephard et al., 2011) and regionally (Beer et al., 2008; Clarisse et al., 2010; Cady-Pereira et al., 2013). These satellite observations have been initially evaluated with in-situ ammonia surface observations. Comparisons of instantaneous twice daily satellite boundary layer averaged observations with footprints on the order of 5–15 km with commonly measured in-situ bi-weekly averaged surface network observations can be challenging given the obvious sampling differences (horizontal, temporal, and vertical). Nevertheless, Pinder et al. (2011) was able to show that the TES ammonia observations reflect spatial gradients and seasonal trends when compared with overlapping bi-weekly CAMNet in-situ surface observations.

Satellite observations of tropospheric ammonia are also contributing to better understanding of the ammonia emission inventories used in chemical transport models. Both IASI and TES satellite observations have been used to evaluate and improve ammonia emissions and transport in global (GEOS-Chem) and regional chemistry transport (Community Multiscale Air Quality (CMAQ)) models, which have been broadly under-predicting ammonia concentrations compared to the satellite observations, especially in large source regions like the Central Valley in California, USA. Some examples include using TES ammonia observations to provide top-down constraints on  $\text{NH}_3$  emissions in GEOS-Chem (Zhu et al., 2012). Recent work by Heald et al. (2012) using IASI observations along with the GEOS-Chem chemical transport model to show that  $\text{NH}_3$  is likely underestimated in California, leading to a local underestimate of ammonium nitrate aerosol. At the same time, Walker et al. (2012) using TES observations showed a similar under prediction of ammonia emissions by GEOS-Chem over California, which has among the largest concentrations of ammonia in the USA. TES satellite and in-situ observations were also used to evaluate the new treatment of ammonia bidirectional fluxes in the CMAQ and GEOS-Chem models (Jeong et al., 2014; Zhu et al., 2014). In addition, insights into the diurnal variability of animal  $\text{NH}_3$  emissions have been obtained by combining TES satellite with in-situ ground-based and aircraft observations

[Title Page](#)[Abstract](#)[Introduction](#)[Conclusions](#)[References](#)[Tables](#)[Figures](#)[|◀](#)[▶|](#)[◀](#)[▶](#)[Back](#)[Close](#)[Full Screen / Esc](#)[Printer-friendly Version](#)[Interactive Discussion](#)

**CrlS satellite observations of NH<sub>3</sub>**

M. W. Shephard and  
K. E. Cady-Pereira

[Title Page](#)[Abstract](#)[Introduction](#)[Conclusions](#)[References](#)[Tables](#)[Figures](#)[|◀](#)[▶|](#)[◀](#)[▶](#)[Back](#)[Close](#)[Full Screen / Esc](#)[Printer-friendly Version](#)[Interactive Discussion](#)

in order to development and evaluated a new improved NH<sub>3</sub> temporal emissions profile for CMAQ (Bash et al., 2014).

While these initial studies have greatly improved our knowledge of the magnitude, seasonal cycle, and spatial distribution of NH<sub>3</sub> emissions, there still remain large uncertainties in ammonia emissions and in the nitrogen cycle in general. Therefore, advancements in our understanding of ammonia emission around the globe will benefit from recent and new satellite ammonia observations. The Cross-track Infrared Sounder (CrlS) instrument is an FTS operated by the USA NOAA/NASA/DoD Joint Polar Satellite System (JPSS) program on Suomi National Polar-orbiting Partnership (NPP) satellite, which was launched on 28 October 2011. With its good radiometric calibration and SNR, CrlS also has the potential to globally monitor ammonia and to contribute to a better understanding of tropospheric ammonia variability over the globe. The overall objective of this analysis is to demonstrate the capability of the CrlS instrument to retrieve atmospheric ammonia. Presented is the CrlS ammonia: (i) retrieval strategy including spectral micowindows and error analysis, (ii) simulations showing the retrieval vertical sensitivity, level-of-detectability, and performance, (iii) and example of the first CrlS observations of elevated ammonia over the Central Valley of California USA, and (iv) initial comparison of these CrlS NH<sub>3</sub> retrievals with coincident TES satellite, Quantum Cascade-Laser (QCL) surface observations (Miller et al., 2014).

## 2 Satellite tropospheric ammonia observations

The main governing satellite sensor characteristics for detecting ammonia in the infrared are the measurement noise, spectral resolution, and local overpass sampling time (as the thermal contrast is tightly correlated with the diurnal cycle). Provided in this section are the CrlS instrument specifications pertinent to ammonia observations, plus a summary of comparable FTS IASI and TES sensor specifications and corresponding ammonia measurement characteristics.

**CrlS satellite observations of NH<sub>3</sub>**

M. W. Shephard and  
K. E. Cady-Pereira

[Title Page](#)

[Abstract](#)

[Introduction](#)

[Conclusions](#)

[References](#)

[Tables](#)

[Figures](#)

◀

▶

◀

▶

[Back](#)

[Close](#)

[Full Screen / Esc](#)

[Printer-friendly Version](#)

[Interactive Discussion](#)



## 2.1 Relevant instrument characteristics

### 2.1.1 Cross-track Infrared Sounder (CrlS)

CrlS is in a sun-synchronous orbit (824 km) with a mean local daytime overpass time of 13:30 mean local solar time in the ascending node, and a mean local nighttime overpass time of 01:30 in the descending node. CrlS provides soundings of the atmosphere over 3 wavelength bands in the infrared. For ammonia retrievals we focus on the 9.14–15.38 μm (650–1095 cm<sup>-1</sup>) range, as NH<sub>3</sub> main infrared absorbing spectral region is between 960 and 970 cm<sup>-1</sup>. In this spectral region CrlS's spectral resolution is 0.625 cm<sup>-1</sup> (Tobin, 2012). CrlS is a across track scanning instrument with a 2200 km swath width ( $\pm 50^\circ$ ) with the total angular field of view consisting of a 3 × 3 array of circular pixels of 14 km diameter each (nadir spatial resolution). While the spectral and spatial resolution of CrlS is less fine than that of TES, its across track scanning swath provides greater spatial coverage which is more similar to IASI. CrlS with a spectral resolution similar to IASI, and ~ 4 times decrease in spectral noise (~ 0.04 at 280 K) in the ammonia spectral region (Zavyalov et al., 2013), has the potential to detect smaller NH<sub>3</sub> concentrations than is currently possible with IASI. For example, the Clarisse et al. (2010) sensitivity study showed that “a reduction of the IASI noise by a factor of 2 (equally 0.1 K) would significantly improve the sensitivity to NH<sub>3</sub> and boundary sensitivity would start at zero thermal contrast during the daytime”.

### 2.1.2 Infrared Atmospheric Sounder Interferometer (IASI)

IASI is an FTS instrument launched in a sun-synchronous orbit with overpass times of 09:30 and 21:30 mean local solar time. It measures thermal infrared radiation in the spectral range from 645–2760 cm<sup>-1</sup> with a spectral resolution 0.5 cm<sup>-1</sup> apodized and noise of ~ 0.15–0.2 K at 280 K at 950 cm<sup>-1</sup>. IASI is a scanning instrument with a 2400 km swath made up of 2 × 2 arrays of 12 km diameter pixels. Under conditions of elevated ammonia amounts and favourable thermal contrast, IASI has peak sensitivity

to atmospheric ammonia in the boundary layer with a lower bound minimum detection threshold of profiles with a surface value of  $\sim 3$  ppbv under atmospheric states with large thermal contrasts (Clarisso et al., 2010).

### 2.1.3 Tropospheric Emission Spectrometer (TES)

- 5 TES has less dense spatial coverage than the scanning satellites (e.g. IASI, CrIS), but has a higher spectral resolution of  $0.06\text{ cm}^{-1}$ . TES is in a sun-synchronous orbit that has both a daytime ascending orbit with a local overpass time of 13:30 mean solar time, providing favorable conditions for high thermal contrast and thus increased sensitivity to boundary layer  $\text{NH}_3$  (Clarisso et al., 2010), and a nighttime descending orbit with  
10 a corresponding 01:30 mean local solar overpass time. The smaller satellite footprint of TES ( $5 \times 8\text{ km}$ ) also allows for the potential to detect more localized  $\text{NH}_3$  sources. The TES instrument has good signal-to-noise (SNR) of  $\sim 0.1\text{--}0.2\text{ K}$  at  $280\text{ K}$  in the  $\text{NH}_3$  region (Worden et al., 2006; Shephard et al., 2008), which is similar to IASI. It also has relative radiometric calibration that is stable over time (Conner et al., 2011), which is  
15 important for long-term trend studies. The combination of the high spectral resolution and good SNR of the TES instrument in the  $\text{NH}_3$  region provides increased sensitivity to  $\text{NH}_3$  mixing ratios near the surface from satellite observations and the selection of spectral regions (microwindows) that reduce the impact of interfering species, and consequently systematic errors in the retrievals. Shephard et al. (2011) showed that  
20 the TES  $\text{NH}_3$  retrievals have (i) a minimum detection level of  $\sim 0.4\text{ ppb RMVR}$ , which corresponds to a profile with a surface mixing ratio of  $\sim 1\text{ ppb}$ , and (ii) typically have peak sensitivity in the boundary layer between  $900\text{--}700\text{ hPa}$  (1–3 km).

## CrIS satellite observations of $\text{NH}_3$

M. W. Shephard and  
K. E. Cady-Pereira

[Title Page](#)

[Abstract](#)

[Introduction](#)

[Conclusions](#)

[References](#)

[Tables](#)

[Figures](#)

◀

▶

◀

▶

[Back](#)

[Close](#)

[Full Screen / Esc](#)

[Printer-friendly Version](#)

[Interactive Discussion](#)



### 3 Retrieval strategy

#### 3.1 NH<sub>3</sub> retrieval methodology

The ammonia retrieval strategy used here follows closely the TES NH<sub>3</sub> retrieval approach (Shephard et al., 2011). It is based on an optimal estimation approach that minimizes the difference between the observed spectral radiances and a nonlinear radiative transfer model driven by the atmospheric state, subject to the constraint that the estimated state must be consistent with an a priori probability distribution for that state (Rodgers, 2000). If the estimated retrieved state,  $\hat{x}$ , is close to the actual true state,  $x$ , then it can be expressed through a linear retrieval as:

$$10 \quad \hat{x} = x_a + \mathbf{A}(x - x_a) + \mathbf{G}\mathbf{n} + \mathbf{GK}_b(b - b_a) \quad (1)$$

where,  $x_a$  is the a priori constraint vector. A priori information is a necessity as the retrieval is an ill-posed problem (can have many potential solutions). For these ammonia retrievals the retrieved profile values are expressed as the natural logarithm of the volume mixing ratio (VMR), since the values span many orders of magnitude in the vertical.  $\mathbf{G}$  is the gain matrix (or “contribution function matrix”) describing the sensitivity of the retrieval to the measurements (and thus measurement error), which maps from measurement (spectral radiance) space into retrieval space. The vector  $\mathbf{n}$  represents the noise on the spectral radiances. The vector  $b$  contains non-retrieved parameters that affect the modeled radiance (e.g., concentrations of interfering gases) that are not included in the retrieved state vector.  $b_a$  holds the corresponding a priori values, and  $\mathbf{K}_b = \partial\mathbf{L}/\partial b$  is the Jacobian describing the dependency of the forward model radiance,  $\mathbf{L}$ , on the vector  $b$ . The fast forward model OSS-CrIS (Moncet et al., 2008), which is built from the Line-By-Line Radiative Transfer Model (LBLRTM) (Clough et al., 2005; Shephard et al., 2009; Alvarado et al., 2013), is used for these retrievals.

25 The averaging kernel,  $\mathbf{A}$ , describes the sensitivity of the retrieval to the true state:

$$\mathbf{A} = \frac{\partial \hat{x}}{\partial x} = \left( \mathbf{K}^T \mathbf{S}_n^{-1} \mathbf{K} + \mathbf{S}_a^{-1} \right)^{-1} \mathbf{K}^T \mathbf{S}_n^{-1} \mathbf{K} = \mathbf{GK} \quad (2)$$

Title Page

Abstract

Introduction

Conclusions

References

Tables

Figures

|◀

▶|

◀

▶

Back

Close

Full Screen / Esc

Printer-friendly Version

Interactive Discussion



The Jacobian  $\mathbf{K}$  (sometimes also called the “weighting function”) describes the sensitivity of the forward model radiances to the state vector ( $\mathbf{K} = \partial\mathbf{L}/\partial\mathbf{x}$ ).  $\mathbf{S}_n$  is the noise covariance matrix, representing the noise in the measured radiances, and  $\mathbf{S}_a$  is the a priori covariance matrix for the retrieval. For profile retrievals, the rows of  $\mathbf{A}$  are functions with some finite width that give a measure of the vertical resolution of the retrieval.  
5 The sum of each row of  $\mathbf{A}$  represents an estimate of the fraction of retrieval information that comes from the measurement rather than the a priori (Rodgers, 2000) at the corresponding altitude, provided the retrieval is relatively linear. The trace of the averaging kernel matrix gives the number of degrees of freedom for signal (DOFS) from the retrieval.  
10

Implemented for these retrievals is an iterative maximum likelihood solution using the Levenberg–Marquardt method strategy (i.e. Clough et al., 1995; Rodgers, 2000):

$$\mathbf{x}^{n+1} = \mathbf{x}^n + \left( \mathbf{K}^T \mathbf{S}_n^{-1} \mathbf{K} + \mathbf{S}_a^{-1} + \left\{ \gamma \mathbf{S}_a^{-1} \right\} \right)^{-1} \mathbf{K}^T \mathbf{S}_n^{-1} [\mathbf{R} - \mathbf{L}] + \mathbf{S}_a^{-1} (\mathbf{x}^a - \mathbf{x}^n) \quad (3)$$

where,  $\left\{ \gamma \mathbf{S}_a^{-1} \right\}$  is the Levenberg–Marquardt term with  $\gamma$  being the Levenberg–Marquardt parameter or penalty function.  $\mathbf{R}$  is the measured spectral radiances from the sensor (i.e. CrIS), and the  $[\mathbf{R} - \mathbf{L}]$  is the spectral residuals being minimized in the retrieval. This numerical iterative approach is needed to account for the nonlinearities in the forward model spectral radiance calculations of the atmospheric state. Without the Levenberg–Marquardt term, this method will generally only be satisfactory  
15 for problems where the residuals are small and the initial guess is sufficiently close to the solution (linear region). Implementing the Levenberg–Marquardt method provides checks when the initial guess does not satisfy this condition from one iterative step to the next, and then only minimizes the cost function over a “trust region” in which the retrieval is considered linear with respect to the step size, before proceeding to the next  
20 iteration step (Bowman et al., 2006; Moré, 1977).  
25

[Title Page](#)[Abstract](#)[Introduction](#)[Conclusions](#)[References](#)[Tables](#)[Figures](#)[◀](#)[▶](#)[◀](#)[▶](#)[Back](#)[Close](#)[Full Screen / Esc](#)[Printer-friendly Version](#)[Interactive Discussion](#)

## 3.2 CrIS NH<sub>3</sub> microwindows

It is often desired to perform the retrievals in spectral regions that are dominated by the species of interest. Determining the spectral regions in which to perform the retrievals (referred to as microwindows if over small spectral domains) can depend on a number of factors. However, the general goal is to obtain the maximum amount of information content while minimizing the impact of systematic errors such as from cross-state interfering species and spectroscopic line parameters errors (laboratory measured spectroscopy lines may have different uncertainties) (Worden et al., 2004). Section 3.3 shows the spectral region used for the CrIS NH<sub>3</sub> retrievals. For the long-wave infrared this is considered a relatively “clean” window region in terms of contributions from strong spectroscopic lines. However, as shown in Sect. 3.3, there is still the potential impact from a number of species such as H<sub>2</sub>O, CO<sub>2</sub>, and O<sub>3</sub> that need to be considered in terms of selection of NH<sub>3</sub> spectroscopic retrieval regions. The column amounts used in the simulated spectrum are provided in Table 1. Utilizing microwindows can also have a practical advantage of reducing the computational burden of the high-spectral resolution forward model calculations, and the storage size of output retrieval parameters (i.e. Jacobians).

## 3.3 A priori vector and constraints

The a priori profiles (vectors) and constraints are those built for the TES NH<sub>3</sub> retrievals (Shephard et al., 2011). In summary, both the a priori profiles and covariance matrices are derived from global distributions of NH<sub>3</sub> from the chemical transport model GEOS-Chem (Zhu et al., 2013) for three categories of NH<sub>3</sub> profiles:

- *Polluted*: represents all profiles with surface NH<sub>3</sub> ≥ 5 ppbv.
- *Moderately polluted*: represents all profiles with 1 ppbv ≥ NH<sub>3</sub> < 5 ppbv at the surface or NH<sub>3</sub> < 1 ppbv at the surface, but NH<sub>3</sub> > 1 ppbv between the surface and

AMTD

7, 11379–11413, 2014

## CrIS satellite observations of NH<sub>3</sub>

M. W. Shephard and  
K. E. Cady-Pereira

[Title Page](#)

[Abstract](#)

[Introduction](#)

[Conclusions](#)

[References](#)

[Tables](#)

[Figures](#)

◀

▶

◀

▶

[Back](#)

[Close](#)

[Full Screen / Esc](#)

[Printer-friendly Version](#)

[Interactive Discussion](#)



500 hPa; this profile type seeks to represent those cases in which the local emissions are less than the important transport into the region.

- *Unpolluted*: all profiles with  $\text{NH}_3 < 1 \text{ ppbv}$  between the surface and 800 hPa.

Since the  $\text{NH}_3$  concentrations are highly variable in time and space, and not well

- 5 known globally from target scene-to-scene, we followed the same two parameter a priori selection algorithm developed for TES. The selection algorithm uses the scene signal-to-noise ratio (SNR) of the CrIS  $\text{NH}_3$  infrared spectral signature and the thermal contrast between the surface and the bottom level of the atmosphere (see Shephard et al. (2011) for further details).

## 10 4 Comparison methodology

One thing that needs to be considered when comparing infrared satellite inferred retrieved profiles for species with limited information, such as ammonia, is that the true vertical resolution of the retrieved parameter is often more coarse than the reported retrieval vertical levels. One of the main reasons for performing retrievals at more levels

- 15 then there is independent pieces of information is to capture the vertical sensitivity as it varies from profile-to-profile depending on the atmospheric state. However, due to this “oversampling”, the minor trace gas species (i.e.  $\text{NH}_3$ ) profiles often have several levels that are substantially influenced by the a priori profile (i.e. containing little information from the measurement). Depending on the purpose of the comparison, or the quantity
- 20 the satellite retrieved observations are being compared against, there are a number of possible satellite comparison methods that can be implemented that take into account the true satellite retrieval sensitivity.

One approach often utilized when comparing the retrieved satellite profile,  $x_c$ , against other profiles is to “map” the comparison data to the satellite levels using a linear weighted average and applying the TES averaging kernel and the a priori to the

[Title Page](#)

[Abstract](#)

[Introduction](#)

[Conclusions](#)

[References](#)

[Tables](#)

[Figures](#)

◀

▶

◀

▶

[Back](#)

[Close](#)

[Full Screen / Esc](#)

[Printer-friendly Version](#)

[Interactive Discussion](#)



[Title Page](#)[Abstract](#)[Introduction](#)[Conclusions](#)[References](#)[Tables](#)[Figures](#)[|](#)[|](#)[◀](#)[▶](#)[Back](#)[Close](#)[Full Screen / Esc](#)[Printer-friendly Version](#)[Interactive Discussion](#)

mapped in situ profile:

$$\mathbf{x}_c^{\text{est}} = \mathbf{x}_a + \mathbf{A} (\mathbf{x}_c^{\text{mapped}} - \mathbf{x}_a) \quad (4)$$

- This comparison approach accounts for the satellite retrieval a priori bias and the sensitivity and vertical resolution by apply the satellites averaging kernel,  $\mathbf{A}$ , and a priori,  $\mathbf{x}_a$ , to the comparison profile  $\mathbf{x}_c^{\text{mapped}}$  (i.e. model or in-situ). This method obtains an estimated profile,  $\mathbf{x}_c^{\text{ext}}$ , that represents what the satellite would measure for the same air mass sampled by the in situ measurements or model. Differences between  $\mathbf{x}_c^{\text{ext}}$  and  $\hat{\mathbf{x}}$  are presumed to be associated with the satellite measurement error on the retrieval and systematic errors resulting from parameters that were not well represented in the forward model (e.g. temperature, interfering gases, and instrument calibration), which are the latter two terms in Eq. (1). This procedure is used to compare the simulated modeled NH<sub>3</sub> profiles with the satellite retrieved profiles.

## 5 Retrieval error analysis

- One advantage of the optimal estimation retrieval approach is that a retrieval error estimate can be computed in a straightforward manner based on retrieval input parameters. The total error covariance matrix  $\mathbf{S}_x$  for a given parameter  $x$  on the retrieved levels  $i$  is given by:

$$\mathbf{S}_x = \underbrace{(\mathbf{A} - \mathbf{I})\mathbf{S}_a(\mathbf{A} - \mathbf{I})^T}_{\text{smoothing}} + \underbrace{\mathbf{G}\mathbf{S}_n\mathbf{G}^T}_{\text{measurement}} + \underbrace{\sum_i \mathbf{G}\mathbf{K}_b^i \mathbf{S}_b (\mathbf{G}\mathbf{K}_b^i)^T}_{\text{systematic + cross state}} \quad (5)$$

- where  $\mathbf{S}_b$  is the expected covariance of the non-retrieved parameters errors (Worden et al., 2004). This total error on the retrieved parameters is expressed as the sum of the smoothing (sometimes referred to as the “representation”) error (first term), the

measurement error (middle term), and the systematic error (last term). The smoothing error is the uncertainty due to unresolved fine structure in the profile. The measurement error is the random instrument noise in the radiance spectrum propagated to the retrieval parameter,  $x$ . The systematic errors are any errors from uncertainties in the non-retrieved forward model parameters, some of which are systematic (i.e. errors in spectroscopic line parameters), and some of which change from cross-state errors propagated from retrieval-to-retrieval (i.e. interfering species). The observation error is defined as a sum of the measurement and systematic plus cross state terms (last two terms in Eq. 5), which is useful to report when the smoothing error is accounted for in a comparison (e.g. assimilations, profile comparisons when the observational operator has been applied, see Sect. 4). Note for this initial study we did not include any systematic errors (last term) in the total error estimates. Thus, the reported total random error covariance matrix, which is just the sum of the first two terms in Eq. (5), can be rearranged and simply written as the inverse of the Hessian,  $H$ ,

$$S_x = H^{-1} = \left( K^T S_n^{-1} K + S_a^{-1} \right)^{-1} \quad (6)$$

## 6 Results

CrlS simulations are utilized to test the algorithm development and to determine the retrieval performance capabilities and characteristics. The CrlS NH<sub>3</sub> retrieval algorithm is then applied to example CrlS observations over the San Joaquin Valley in California, USA and compared with nearby TES satellite and Quantum Cascade-Laser-based (QCL) surface observations (Miller et al., 2014).

### 6.1 CrlS simulations

To evaluate the performance of the CrlS NH<sub>3</sub> retrieval over a range of atmospheric conditions we used simulated data where the truth is known. We utilized the modelled

## CrlS satellite observations of NH<sub>3</sub>

M. W. Shephard and  
K. E. Cady-Pereira

[Title Page](#)

[Abstract](#)

[Introduction](#)

[Conclusions](#)

[References](#)

[Tables](#)

[Figures](#)

◀

▶

◀

▶

[Back](#)

[Close](#)

[Full Screen / Esc](#)

[Printer-friendly Version](#)

[Interactive Discussion](#)



ammonia simulated database as in Shephard et al. (2011) for the TES retrieval evaluation. This simulated data set consisted of GEOS-Chem NH<sub>3</sub> profiles (with double the NH<sub>3</sub> emissions) that are matched up with representative atmospheric states over central US during July 2005. In order to better expand the full retrieval space the NH<sub>3</sub> concentrations were increased by an additional factor of 2 from the profile values in Shephard et al. (2011) and raising the number of simulated profiles to 400. These atmospheric states were then inserted into the radiative transfer forward model to generate upwelling spectral radiances. The CrIS estimated measurement noise (random) was subsequently added to each spectrum to generate the CrIS simulated spectral radiances. These CrIS simulated spectral radiances were used with the retrieval strategy and methodology outlined in Sect. 3 in order to evaluate the capabilities of the CrIS NH<sub>3</sub> retrieval.

### 6.1.1 CrIS retrieval performance

This simulated dataset produced the CrIS NH<sub>3</sub> retrieved profiles shown in Fig. 2. The maximum number of valid retrieved values from any retrieval level used in the comparison was 109. The profile comparisons differences (retrieval – true) were performed using Eq. (4), which removes the influence of the retrieval a priori from the comparison. More specific statistical insight can be gained by binning the results in Fig. 2 by pressure as shown in Fig. 3. The statistics were performed on levels containing some sensitivity (sum of the rows of the averaging kernel > 0.3), which is a balance between including values with the most information while still retaining enough values for reliable statistical inference. The CrIS retrieval strategy works well with a median bias of ~ 6 % (ranging from 3 to 8 %), with variability of -4 % (ranging from 0 to -10 % for the 25th quartile) to +26 % (ranging from +14 to +39 % for the 75th quartile). These actual errors should be treated as lower bounds considering the ideal simulated conditions where full atmospheric state besides NH<sub>3</sub> is known perfectly. The sum of the rows of the averaging kernels show that on average the peak sensitive in the vertical region from ~ 850–750 hPa (~ 1.5 to 2.5 km).

## CrIS satellite observations of NH<sub>3</sub>

M. W. Shephard and  
K. E. Cady-Pereira

[Title Page](#)

[Abstract](#)

[Introduction](#)

[Conclusions](#)

[References](#)

[Tables](#)

[Figures](#)

◀

▶

◀

▶

[Back](#)

[Close](#)

[Full Screen / Esc](#)

[Printer-friendly Version](#)

[Interactive Discussion](#)



## 6.1.2 CrIS minimum detection threshold

### CrIS satellite observations of NH<sub>3</sub>

M. W. Shephard and  
K. E. Cady-Pereira

[Title Page](#)

[Abstract](#)

[Introduction](#)

[Conclusions](#)

[References](#)

[Tables](#)

[Figures](#)

[|◀](#)

[▶|](#)

[◀](#)

[▶](#)

[Back](#)

[Close](#)

[Full Screen / Esc](#)

[Printer-friendly Version](#)

[Interactive Discussion](#)



are provided by looking at the 25th percentile (Q25) peak  $\text{NH}_3$  profile value of 0.9 ppbv (with  $\text{SNR} = 1.6$ ,  $\text{DOFS} = 0.6$ , thermal contrast = 5 K), and the bin's median peak  $\text{NH}_3$  profile value of 1.2 ppbv ( $\text{SNR} = 1.2$ ,  $\text{DOFS} = 0.67$ , thermal contrast = 5 K).

## 6.2 CrIS observations

- To demonstrate the applicability and further evaluate the CrIS retrieval it was then applied to real CrIS observations. For this initial study a region over the San Joaquin Valley in California, USA was selected as this is a region of interest that is known for elevated boundary layer ammonia concentrations and spatial variability in and around the valley (e.g. Beer et al., 2008; Clarisse et al., 2010). Also, during this period there are coincident TES satellite and QCL surface observations (Miller et al., 2014) taken at the same time as NASA's Deriving Information on Surface Conditions from Column and Vertically Resolved Observations Relevant to Air Quality (DISCOVER-AQ) campaign ([http://www.nasa.gov/mission\\_pages/discover-aq/index.html](http://www.nasa.gov/mission_pages/discover-aq/index.html)).

### 6.2.1 Detailed $\text{NH}_3$ profile retrieval example

- Presented here is a detailed analysis of the CrIS measured spectrum and corresponding retrieval results from one of the elevated cases in the San Joaquin Valley region on 28 January 2013. Figure 6 contains the CrIS measured spectra in the ammonia retrieval region reported in brightness temperature. Even under elevated ammonia concentration conditions the ammonia spectral signal is only on the order of 1 K in brightness temperature, which is only  $\sim 0.3\%$  of the total longwave infrared signal. Figure 6 also demonstrates how well the spectral residuals in Fig. 6b ( $(\mathbf{R} - \mathbf{L})$  in Eq. 3) are minimized by the retrieval in Fig. 6c to produce the retrieved  $\text{NH}_3$  profile in Fig. 7 (the  $x$  in Eq. 3) through the retrieval inversion.

- Figure 7 contains the resulting CrIS retrieved  $\text{NH}_3$  profile and the retrieval properties from the 28 January 2013 CrIS example shown in Fig. 6. For this retrieval there is 1 piece of information (reported as the DOFS) provided by the observation. As shown by

AMTD

7, 11379–11413, 2014

## CrIS satellite observations of $\text{NH}_3$

M. W. Shephard and  
K. E. Cady-Pereira

Title Page

Abstract

Introduction

Conclusions

References

Tables

Figures

◀

▶

◀

▶

Back

Close

Full Screen / Esc

Printer-friendly Version

Interactive Discussion



**CrlS satellite observations of NH<sub>3</sub>**

M. W. Shephard and  
K. E. Cady-Pereira

[Title Page](#)

[Abstract](#)

[Introduction](#)

[Conclusions](#)

[References](#)

[Tables](#)

[Figures](#)

◀

▶

◀

▶

[Back](#)

[Close](#)

[Full Screen / Esc](#)

[Printer-friendly Version](#)

[Interactive Discussion](#)



the NH<sub>3</sub> averaging kernels, the information provided by CrlS in this example is in the profile from the surface to 600 hPa, with the peak sensitivity in the 900–800 hPa range. The retrieved profile shows high ammonia amounts with values of 11 ppbv at 825 hPa where the averaging kernels show the peak CrlS retrieval sensitivity.

A nearby TES retrieval corresponding to the CrlS profile in Fig. 7 is provided in Fig. 8 for general comparison purposes. Comparing these two retrievals the TES retrieval tends to have increased sensitivity lower down in the troposphere compared with the CrlS retrieval. Also, the CrlS retrieval tends to retrieve higher values of NH<sub>3</sub> compared with the nearby TES retrieval. The estimated total retrieval errors in this case are relatively large at ~ 40–50 % for both the CrlS and TES retrievals. A more detailed comparison of CrlS with both TES and the QCL are provided in the following section.

### 6.2.2 Central Valley comparisons with TES and QCL

As part of the DISCOVER-AQ campaign TES performed special observations and the QCL provided in-situ surface observations in the Central Valley in California, USA. On

28 January 2013 TES performed a transect (Run 16444) that consisted of 20 contiguous high spatial density 12 km samples that transected over ~ 240 km section of the Central Valley from 21:24:55 to 21:27:58 UTC. During DISCOVER-AQ QCL measurements were taken to match up as close as possible to the TES transect path. The CrlS measurements are selected around the TES transect. Figure 9 contains an overlay of the CrlS (large circles), TES (rectangles), and the QCL (small circles) over the Central Valley region covered by the QCL. Since the CrlS and TES retrievals were performed with the same retrieval algorithm at the same pressure levels and with the same a priori information, for these comparisons we opted to show the satellite results from 900 hPa, which is generally the retrieval level with the peak vertical sensitivity (as shown in Fig. 10). Since the satellite and QCL measurements are sampling different parts of the lower boundary layer direct absolute satellite comparisons are not possible. Note, that the QCL surface measurements are scaled by 1/6 for the comparison. However, relative comparisons along the transect do provide valuable insights into the

<a href="#">Title Page</a>	
<a href="#">Abstract</a>	<a href="#">Introduction</a>
<a href="#">Conclusions</a>	<a href="#">References</a>
<a href="#">Tables</a>	<a href="#">Figures</a>
<a href="#">◀</a>	<a href="#">▶</a>
<a href="#">◀</a>	<a href="#">▶</a>
<a href="#">Back</a>	<a href="#">Close</a>
<a href="#">Full Screen / Esc</a>	
<a href="#">Printer-friendly Version</a>	
<a href="#">Interactive Discussion</a>	

performance of the satellite retrievals. Note the large spatial fluctuations in the surface QCL NH<sub>3</sub> observations as the instrument was driven on roads around this region aligned closely to the TES transect. The spatial map in Fig. 9 shows good agreement between all three observations in terms of general regions of higher and lower NH<sub>3</sub> concentrations.

More details on the comparison shown in Fig. 9 are provided in Fig. 10. Here it is seen that in general the atmospheric conditions on 28 January 2013 were favourable for ammonia satellite retrievals with thermal contrasts > 6 K, relatively high ammonia concentrations, and most of the transect sufficiently free of thick clouds. The exception is the southerly most region of the transect where the clouds optical depths (COD) approach 1, which is sufficiently thick to block out the ammonia atmospheric signal (Shephard et al., 2011). Most of this transect had conditions that resulted in the degrees of freedom for the TES observations being ~ 1. The peak vertical sensitivity is around 1 km (900 hPa), with CrIS sometimes having its peak sensitivity as high as ~ 2.5 km (750 hPa). For comparison purposes the high temporal measurements of the QCL were smoothed by a running boxcar computing median values; the boxcar width matched the spatial sampling of the TES observations. Even though ammonia can be extremely variable in both space and time (as depicted by the QCL), and the horizontal and vertical sampling of the in-situ and satellite observations are very different, CrIS and TES satellite observations qualitatively captures the general variations seen in the surface in-situ ammonia concentrations. Also, the TES and CrIS satellite observations themselves quantitatively agree very well and are often within the uncertainty bars of the two instruments. In general the satellite retrieved NH<sub>3</sub> values tends to be slightly larger from CrIS than TES.

## 25 7 Conclusions

This study presents a robust CrIS NH<sub>3</sub> retrieval that demonstrates the capabilities of utilizing CrIS to measure tropospheric ammonia. Based on both CrIS simulations and



real observation there are a number of insights gained in terms of the ability of CrIS to measure tropospheric ammonia. The peak CrIS sensitivity to  $\text{NH}_3$  is in the “boundary layer” and range from 900–750 hPa ( $\sim 1.0\text{--}2.5$  km). It has a minimum  $\text{NH}_3$  detection limit of  $\sim 1$  ppbv. The retrievals have limited information content with most 1 piece of information (DOFS), which provides more of an average boundary layer mixing ratio value (or a partial column type) measurement as opposed to a true atmospheric  $\text{NH}_3$  profile, which would have a number of independent pieces of information in the vertical. The information content and sensitivity varies from profile-to-profile depending on the atmospheric conditions, with increased thermal contrast and ammonia concentrations providing improved measurement sensitivity. The retrieval performance based on simulations where the truth is known shows a small positive bias of  $\sim 6\%$  with a variability ranging from  $-4$  to  $26\%$  (defined by the 25th and 75th percentiles). Considering these are ideal conditions where everything except the ammonia is known perfectly, these should be considered as lower bounds on the actual errors.

Retrievals from CrIS observations on 28 January 2013 during the DISCOVER-AQ field study over the Central Valley in California, USA demonstrates the sensors ability to capture the general spatial gradient observed by nearby QCL and TES observations. CrIS values at  $\sim 1$  km compare very well with the TES observations, and the differences are generally within the error estimates.

There are a number of refinements to the retrieval strategy that will be addressed in the future to facilitate more routine operational global CrIS retrievals. Some of these potential improvements include: (i) accounting for impact of clouds on the  $\text{NH}_3$  retrieval (Shephard et al., 2011) either through screening, or more desirably retrieving the clouds (Kulawik et al., 2006; Eldering et al., 2008), (ii) further exploring the impact of interfering species (i.e. water vapour) on systematic errors on the ammonia retrieval as CrIS has a  $0.625\text{ cm}^{-1}$  spectral resolution, (iii) refinement of the CrIS surface property retrievals (i.e. surface temperature and emissivity) in the ammonia spectral region to further reduce their impact on the ammonia retrievals.

## CrIS satellite observations of $\text{NH}_3$

M. W. Shephard and  
K. E. Cady-Pereira

[Title Page](#)

[Abstract](#)

[Introduction](#)

[Conclusions](#)

[References](#)

[Tables](#)

[Figures](#)

[|◀](#)

[▶|](#)

[◀](#)

[▶](#)

[Back](#)

[Close](#)

[Full Screen / Esc](#)

[Printer-friendly Version](#)

[Interactive Discussion](#)



*Acknowledgements.* We would like to thank the DISCOVER-AQ 2013 California campaign, especially Princeton's Atmospheric Chemistry Group of Kang Sun, David Miller, and Mark Zondlo for providing the QCL surface data. Funding support for the QCL sensor is from the National Science Foundation Grant #ECC-0540832, and the corresponding QCL validation support is provided by a NASA Earth and Space Science Fellowship #NN12AN64H. We would also like to acknowledge the Atmospheric and Environmental Research (AER) CrIS science team for providing valuable insight in the operational CrIS observations and retrievals, in particular Richard Lynch, Gennady Uymin, and Jean-Luc Moncet. This work at AER was supported under Grant #NA130AR4310060 from the NOAA Climate Program Office (CPO) Atmospheric Chemistry, Carbon Cycle, and Climate (AC4) program.

## References

- Alvarado, M. J., Payne, V. H., Mlawer, E. J., Uymin, G., Shephard, M. W., Cady-Pereira, K. E., Delamere, J. S., and Moncet, J.-L.: Performance of the Line-By-Line Radiative Transfer Model (LBLRTM) for temperature, water vapor, and trace gas retrievals: recent updates evaluated with IASI case studies, *Atmos. Chem. Phys.*, 13, 6687–6711, doi:10.5194/acp-13-6687-2013, 2013.
- Bash, J., Henze, D. K., Jeong, G.-R., Zhu, L., Cady-Pereira, K. E., Shephard, M. W., Pinder, R. W., and Luo, M.: The impact of the diurnal temporal allocation of ammonia emissions on air-quality model estimates of ambient ammonia and inorganic aerosol, in preparation, 2014.
- Bash, J. O., Henze, D. K., Zhu, L., Jeong, G.-R., Walker, J. T., Nowak, J. B., Neuman, J. A., Cady-Pereira, K. E., Shephard, M. W., Luo, M., and Pinder, R. W.: New insights into the diurnal variability of animal NH<sub>3</sub> emissions using in situ, satellite and aloft observations, AGU Fall Meeting, San Francisco, CA, 12 December 2013.
- Beer, R., Glavich, T., and Rider, D. M.: Tropospheric emission spectrometer for the Earth Observing System's Aura satellite, *Appl. Optics*, 40, 2356–2367, 2001.
- Beer, R., Shephard, M. W., Kulawik, S. S., Clough, S. A., Eldering, A., Bowman, K. W., Sander, S. P., Fisher, B. M., Payne, V. H., Luo, M., Osterman, G. B., and Worden, J. R.: First satellite observations of lower tropospheric ammonia and methanol, *Geophys. Res. Lett.*, 35, L09801, doi:10.1029/2008GL033642, 2008.

<a href="#">Title Page</a>	
<a href="#">Abstract</a>	<a href="#">Introduction</a>
<a href="#">Conclusions</a>	<a href="#">References</a>
<a href="#">Tables</a>	<a href="#">Figures</a>
<a href="#">◀</a>	<a href="#">▶</a>
<a href="#">◀</a>	<a href="#">▶</a>
<a href="#">Back</a>	<a href="#">Close</a>
<a href="#">Full Screen / Esc</a>	
<a href="#">Printer-friendly Version</a>	
<a href="#">Interactive Discussion</a>	



- Bowman, K. W., Rodgers, C. D., Sund-Kulawik, S., Worden, J., Sarkissian, E., Osterman, G., Steck, T., Luo, M., Eldering, A., Shephard, M. W., Worden, H., Clough, S. A., Brown, P. D., Rinsland, C. P., Lampel, M., Gunson, M., and Beer, R.: Tropospheric emission spectrometer: retrieval method and error analysis, *IEEE T. Geosci. Remote*, 44, 1297–1307, doi:10.1109/TGRS.2006.871234, 2006.
- Cady-Pereira, K. E., Shephard, M. W., Millet, D. B., Luo, M., Wells, K. C., Xiao, Y., Payne, V. H., and Worden, J.: Methanol from TES global observations: retrieval algorithm and seasonal and spatial variability, *Atmos. Chem. Phys.*, 12, 8189–8203, doi:10.5194/acp-12-8189-2012, 2012.
- Carfrae, J. A., Sheppard, L. J., Raven, J., Stein, W., Leith, I. D., Theobald, A., and Crossley, A.: Early effects of atmospheric ammonia deposition on *Calluna vulgaris* (L.) hull growing on an ombrotrophic peat bog, *Water Air Soil Pollut. Focus*, 4, 229–239, 2004.
- Charlson, R. J., Langner, J., Rodhe, H., Leovy, C. B., and Warren, S. G.: Perturbation of the Northern-Hemisphere radiative balance by backscattering from anthropogenic sulfate aerosols, *Tellus A*, 43, 152–163, 1991.
- Clarisso, L., Clerbaux, C., Dentener, F., Hurtmans, D., and Coheur, P.-F.: Global ammonia distribution derived from infrared satellite observations, *Nat. Geosci.*, 2, 479–483, doi:10.1038/ngeo551, 2009.
- Clarisso, L., Shephard, M. W., Dentener, F., Hurtmans, D., Cady-Pereira, K., Karagulian, F., Van Damme, M., Clerbaux, C., and Coheur, P.-F.: Satellite monitoring of ammonia: a case study of the San Joaquin Valley, *J. Geophys. Res.*, 115, D13302, doi:10.1029/2009JD013291, 2010.
- Clerbaux, C., Boynard, A., Clarisse, L., George, M., Hadji-Lazaro, J., Herbin, H., Hurtmans, D., Pommier, M., Razavi, A., Turquety, S., Wespes, C., and Coheur, P.-F.: Monitoring of atmospheric composition using the thermal infrared IASI/MetOp sounder, *Atmos. Chem. Phys.*, 9, 6041–6054, doi:10.5194/acp-9-6041-2009, 2009.
- Clough, S. A., Rinsland, C. P., and Brown, P. D.: Retrieval of tropospheric ozone from simulations of nadir spectral radiances as observed from space, *J. Geophys. Res.*, 100, 16579–16593, doi:10.1029/95JD01388, 1995.
- Clough, S. A., Shephard, M. W., Mlawer, E. J., Delamere, J. S., Iacono, M. J., Cady-Pereira, K., Boukabara, S., and Brown, R. D.: Atmospheric radiative transfer modeling: a summary of the AER codes, *J. Quant. Spectrosc. Ra.*, 91, 233–244, 2005.

CrIS satellite observations of NH<sub>3</sub>M. W. Shephard and  
K. E. Cady-Pereira[Title Page](#)[Abstract](#)[Introduction](#)[Conclusions](#)[References](#)[Tables](#)[Figures](#)[|◀](#)[▶|](#)[◀](#)[▶](#)[Back](#)[Close](#)[Full Screen / Esc](#)[Printer-friendly Version](#)[Interactive Discussion](#)

**CrlS satellite observations of NH<sub>3</sub>**M. W. Shephard and  
K. E. Cady-Pereira

Connor, T. C., Shephard, M. W., Payne, V. H., Cady-Pereira, K. E., Kulawik, S. S., Luo, M., Osterman, G., and Lampel, M.: Long-term stability of TES satellite radiance measurements, *Atmos. Meas. Tech.*, 4, 1481–1490, doi:10.5194/amt-4-1481-2011, 2011.

Eldering, A., Kulawik, S. S., Worden, J., Bowman, K., and Osterman, G.: Implementation of cloud retrievals for TES atmospheric retrievals: 2. Characterization of cloud top pressure and effective optical depth retrievals, *J. Geophys. Res.*, 113, D16S37, doi:10.1029/2007JD008858, 2008.

Heald, C. L., Collett Jr., J. L., Lee, T., Benedict, K. B., Schwandner, F. M., Li, Y., Clarisse, L., Hurtmans, D. R., Van Damme, M., Clerbaux, C., Coheur, P.-F., Philip, S., Martin, R. V., and Pye, H. O. T.: Atmospheric ammonia and particulate inorganic nitrogen over the United States, *Atmos. Chem. Phys.*, 12, 10295–10312, doi:10.5194/acp-12-10295-2012, 2012.

Jeong, G.-R., Bash, J. O., Henze, D. K., Pinder, R. W., Walker, J., Cady-Pereira, K., Shephard, M. W., Luo, M., Foley, K. K., Howard, S., and Appel, W. K.: Evaluation of reduced nitrogen with ammonia bidirectional fluxes in CMAQ using in-situ and satellite observations, submitted, 2014.

JPL: TES Level 2 Data User's Guide, edited by: Osterman, G., available at: [http://tes.jpl.nasa.gov/uploadedfiles/TES\\_L2\\_Data\\_Users\\_Guide-1.pdf](http://tes.jpl.nasa.gov/uploadedfiles/TES_L2_Data_Users_Guide-1.pdf) (last access: 2014), 2006.

Kulawik, S. S., Worden, J., Eldering, A., Bowman, K. W., Gunson, M., Osterman, G., Zhang, L., Clough, S. A., Shephard, M. W., and Beer, R.: Implementation of cloud retrievals for Tropospheric Emission Spectrometer (TES) atmospheric retrievals – Part I: Description and characterization of errors on trace gas retrievals, *J. Geophys. Res.*, 111, D24204, doi:10.1029/2005JD006733, 2006.

Lamarque, J.-F., Bond, T. C., Eyring, V., Granier, C., Heil, A., Klimont, Z., Lee, D., Liousse, C., Mieville, A., Owen, B., Schultz, M. G., Shindell, D., Smith, S. J., Stehfest, E., Van Aardenne, J., Cooper, O. R., Kainuma, M., Mahowald, N., McConnell, J. R., Naik, V., Riahi, K., and van Vuuren, D. P.: Historical (1850–2000) gridded anthropogenic and biomass burning emissions of reactive gases and aerosols: methodology and application, *Atmos. Chem. Phys.*, 10, 7017–7039, doi:10.5194/acp-10-7017-2010, 2010.

Miller, D. J., Sun, K., Tao, L., Khan, M. A., and Zondlo, M. A.: Open-path, quantum cascade-laser-based sensor for high-resolution atmospheric ammonia measurements, *Atmos. Meas. Tech.*, 7, 81–93, doi:10.5194/amt-7-81-2014, 2014.

Moncet, J.-L., Uymin, G., Lipton, A. E., and Snell, H. E.: Infrared radiance modeling by optimal spectral sampling, *J. Atmos. Sci.*, 65, 3917–3934, 2008.

[Title Page](#)[Abstract](#)[Introduction](#)[Conclusions](#)[References](#)[Tables](#)[Figures](#)[|◀](#)[▶|](#)[◀](#)[▶](#)[Back](#)[Close](#)[Full Screen / Esc](#)[Printer-friendly Version](#)[Interactive Discussion](#)

## CrlS satellite observations of NH<sub>3</sub>

M. W. Shephard and  
K. E. Cady-Pereira

- Moré, J. J.: The Levenberg–Marquardt algorithm: implementation and theory, in: Proc. Biennial Conf. Numerical Analysis, 105–116, 1977.
- Paerl, H. W., Dennis, R. L., and Whitall, D. R.: Atmospheric deposition of nitrogen: implications for nutrient over-enrichment of coastal waters, *Estuaries*, 24, 667–693, 2002.
- Pinder, R. W., Walker, J. T., Bash, J. O., Cady-Pereira, K. E., Henze, D. K., Luo, M., and Shephard, M. W.: Quantifying spatial and temporal variability in atmospheric ammonia with in situ and space-based observations, *Geophys. Res. Lett.*, 38, L04802, doi:10.1029/2010GL046146, 2011.
- Pope, C. A.: Epidemiology of fine particulate air pollution and human health: biologic mechanisms and who's at risk?, *Environ. Health Persp.*, 108, 713–723, 2000.
- Reay, D. S., Dentener, F., Smith, P., Grace, J., and Feely, R. A.: Global nitrogen deposition and carbon sinks, *Nat. Geosci.*, 1, 430–437, doi:10.1038/ngeo230, 2008.
- Rodgers, C. D.: Inverse Methods For Atmospheric Sounding: Theory and Practice, World Sci., Hackensack, N. J., 2000.
- Seinfeld, J. H. and Pandis, S. N.: Atmospheric Chemistry and Physics, John Wiley, Hoboken, NJ, 1988.
- Shephard, M. W., Worden, H. M., Cady-Pereira, K. E., Lampel, M., Luo, M., Bowman, K. W., Sarkissian, E., Beer, R., Rider, D. M., Tobin, D. C., Revercomb, H. E., Fisher, B. M., Tremblay, D., Clough, S. A., Osterman, G. B., and Gunson, M.: Tropospheric Emission Spectrometer spectral radiance comparisons, *J. Geophys. Res.*, 113, D15S05, doi:10.1029/2007JD008856, 2008.
- Shephard, M. W., Clough, S. A., Payne, V. H., Smith, W. L., Kireev, S., and Cady-Pereira, K. E.: Performance of the line-by-line radiative transfer model (LBLRTM) for temperature and species retrievals: IASI case studies from JAIVEx, *Atmos. Chem. Phys.*, 9, 7397–7417, doi:10.5194/acp-9-7397-2009, 2009.
- Shephard, M. W., Cady-Pereira, K. E., Luo, M., Henze, D. K., Pinder, R. W., Walker, J. T., Rinsland, C. P., Bash, J. O., Zhu, L., Payne, V. H., and Clarisse, L.: TES ammonia retrieval strategy and global observations of the spatial and seasonal variability of ammonia, *Atmos. Chem. Phys.*, 11, 10743–10763, doi:10.5194/acp-11-10743-2011, 2011.
- Tobin, D.: Early checkout of the Cross-track Infrared Sounder (CrlS) on Suomi-NPP, through the atmosphere, Summer 2012, available at: [www.ssec.wisc.edu/news/media/2012/07/ttasummer20121.pdf](http://www.ssec.wisc.edu/news/media/2012/07/ttasummer20121.pdf) (last access: 2014), 2012.

<a href="#">Title Page</a>	<a href="#">Abstract</a>	<a href="#">Introduction</a>
<a href="#">Conclusions</a>	<a href="#">References</a>	
<a href="#">Tables</a>	<a href="#">Figures</a>	
<a href="#">◀</a>	<a href="#">▶</a>	
<a href="#">◀</a>	<a href="#">▶</a>	
<a href="#">Back</a>	<a href="#">Close</a>	
<a href="#">Full Screen / Esc</a>		
	<a href="#">Printer-friendly Version</a>	
	<a href="#">Interactive Discussion</a>	



- Walker, J. M., Philip, S., Martin, R. V., and Seinfeld, J. H.: Simulation of nitrate, sulfate, and ammonium aerosols over the United States, *Atmos. Chem. Phys.*, 12, 11213–11227, doi:10.5194/acp-12-11213-2012, 2012.
- Worden, H., Beer, R., Bowman, K., Fisher, B., Luo, M., Rider, D., Sarkissian, E., Tremblay, D., and Zong, J.: TES level 1 algorithms: interferogram processing, geolocation, radiometric, and spectral calibration, *IEEE T. Geosci. Remote*, 44, 1288–1296, doi:10.1109/TGRS.2005.863717, 2006.
- Worden, J., Kulawik, S. S., Shephard, M. W., Clough, S. A., Worden, H., Bowman, K., and Goldman, A.: Predicted errors of tropospheric emission spectrometer nadir retrievals from spectral window selection, *J. Geophys. Res.*, 109, D09308, doi:10.1029/2004JD004522, 2004.
- Zavyalov, V., Esplin, M., Scott, D., Esplin, B., Bingham, G., Hoffman, E., Lietzke, C., Predina, J., Frain, R., Suwinski, L., Han, Y., Major, C., Graham, B., and Phillips, L.: Noise performance of the CrIS instrument, *J. Geophys. Res.-Atmos.*, 118, 13108–13120, doi:10.1002/2013JD020457, 2013.
- Zhu, L., Henze, D. K., Cady-Pereira, K. E., Shephard, M. W., Luo, M., Pinder, R. W., Bash, J. O., and Jeong, G.: Constraining US ammonia emissions using TES remote sensing observations and the GEOS-Chem adjoint model, *J. Geophys. Res.*, 118, doi:10.1002/jgrd.50166, 2013.
- Zhu, L., Henze, D. K., Bash, J. O., Jeong, G.-R., Cady-Pereira, K. E., Shephard, M. W., Luo, M., Pinder, R. W., Paulot, F., and Capps, S.: Global evaluation of ammonia bi-directional exchange, in preparation, 2014.

**CrIS satellite  
observations of NH<sub>3</sub>**

M. W. Shephard and  
K. E. Cady-Pereira

[Title Page](#)

[Abstract](#)

[Introduction](#)

[Conclusions](#)

[References](#)

[Tables](#)

[Figures](#)

◀

▶

◀

▶

[Back](#)

[Close](#)

[Full Screen / Esc](#)

[Printer-friendly Version](#)

[Interactive Discussion](#)



**CrlS satellite  
observations of NH<sub>3</sub>**M. W. Shephard and  
K. E. Cady-Pereira**Table 1.** Column amounts used in the CrlS simulated forward model calculations in Fig. 1.

Molecule	Background (molec cm <sup>-2</sup> )	Enhanced (molec cm <sup>-2</sup> )
H <sub>2</sub> O	$5.42 \times 10^{22}$	$5.96 \times 10^{22}$
CO <sub>2</sub>	$8.09 \times 10^{21}$	$8.49 \times 10^{21}$
O <sub>3</sub>	$7.35 \times 10^{18}$	$8.08 \times 10^{21}$
NH <sub>3</sub>	$1.05 \times 10^{14}$	$4.91 \times 10^{16}$

[Title Page](#)[Abstract](#)[Introduction](#)[Conclusions](#)[References](#)[Tables](#)[Figures](#)[Back](#)[Close](#)[Full Screen / Esc](#)[Printer-friendly Version](#)[Interactive Discussion](#)

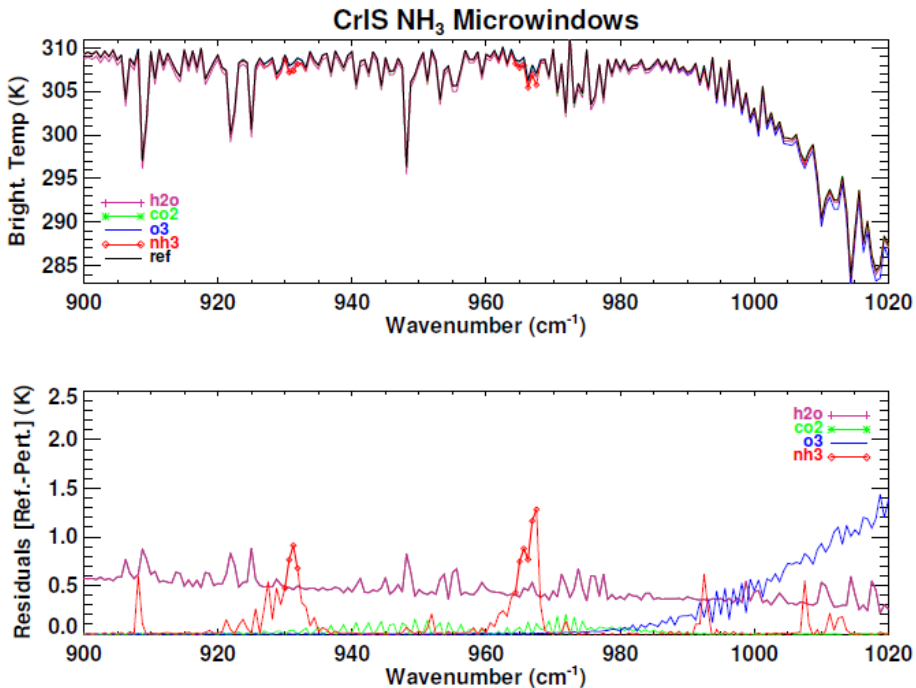


**Figure 1.** Plot of the CrIS spectral microwindow selection for  $\text{NH}_3$  retrievals. The top panel is the model simulated CrIS observation for a reference atmosphere (plotted in black). Overplotted in color are various simulated model calculations computed from the reference atmospheric profile perturbed separately by 10 %  $\text{H}_2\text{O}$ , 10 %  $\text{CO}_2$ , 10 %  $\text{O}_3$ , and  $\text{NH}_3$  increased to a polluted profile. The bottom panel shows the residual (reference–perturbation) TOA brightness temperatures. The diamonds represent spectral points in the  $\text{NH}_3$  microwindows.

## CrIS satellite observations of NH<sub>3</sub>

M. W. Shephard and  
K. E. Cady-Pereira

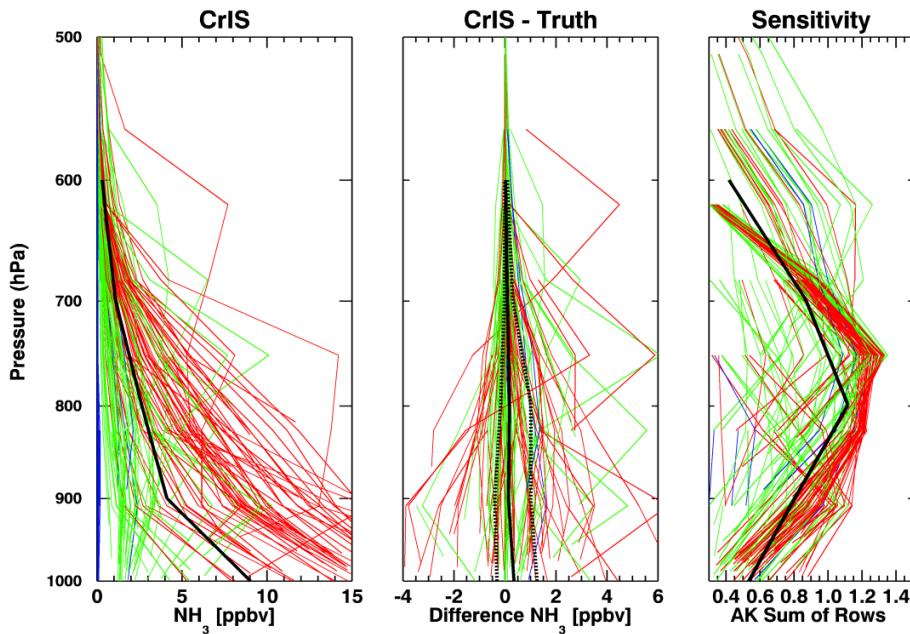


**Figure 2.** Simulated NH<sub>3</sub> retrieval results over the central USA from the July 2005. The thin colors indicate type of true profile: polluted (red), moderate (green), unpolluted (blue). The left panel contains the retrieved profiles, with the black solid line being the median values. The middle panel shows the profile differences (retrieved – truth), where the thick solid black line is median difference and the dashed black lines are the 25th and 75th percent quartiles. The right panel is the sum of the rows of the averaging kernel, with the black line being the median.

## CrlS satellite observations of NH<sub>3</sub>

M. W. Shephard and  
K. E. Cady-Pereira

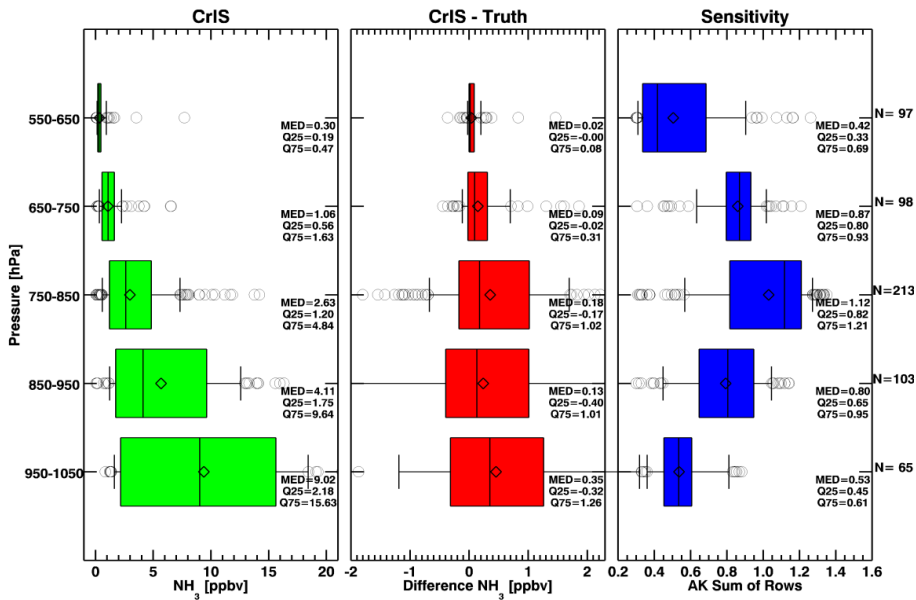


**Figure 3.** General characteristics for the simulated CrIS profile retrievals in Fig. 2 binned by pressure. The boxes edges are the 25th and 75th percentile, the line in the box is the median, the diamond is the mean, the whiskers are the 10th and 90th percentiles, and the circles are the outlier values outside the whiskers.

Title Page

## Abstract

Introduction

## Conclusion

## References

## Table

## Figures

Page

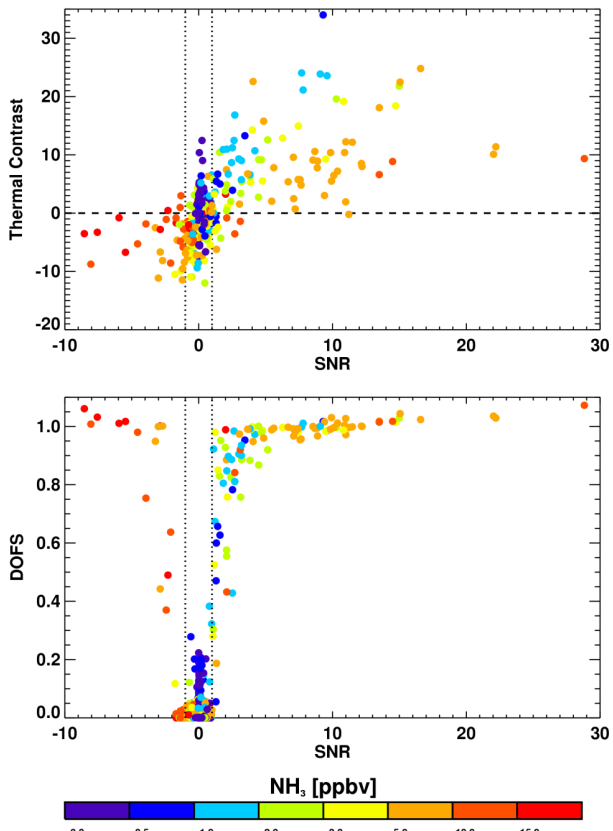
1

Full Screen / Esc

[Printer-friendly Version](#)

## Interactive Discussion

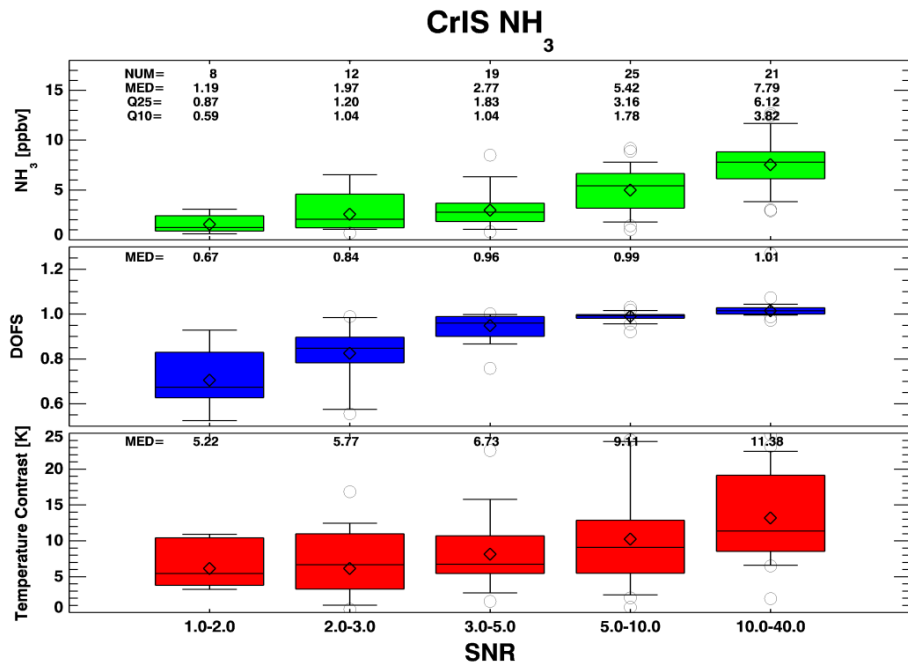




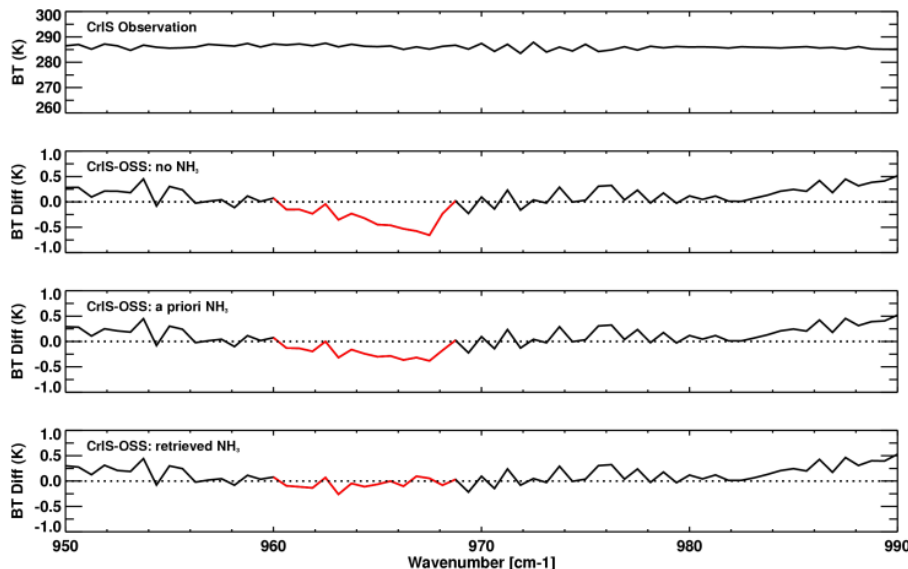
**Figure 4.** Using the same simulated data set as in Fig. 2 the top plot shows the SNR (difference between FM runs with and without NH<sub>3</sub> averaged over the 966.875–967.5 window) vs. thermal contrast, color coded by the peak value of the NH<sub>3</sub> profile. The bottom panel shows the degrees-of-freedom-for-signal (DOFS) vs. NH<sub>3</sub> signal (SNR). The dashed lines just indicate the SNR = 1 threshold.

## CrlS satellite observations of NH<sub>3</sub>

M. W. Shephard and  
K. E. Cady-Pereira

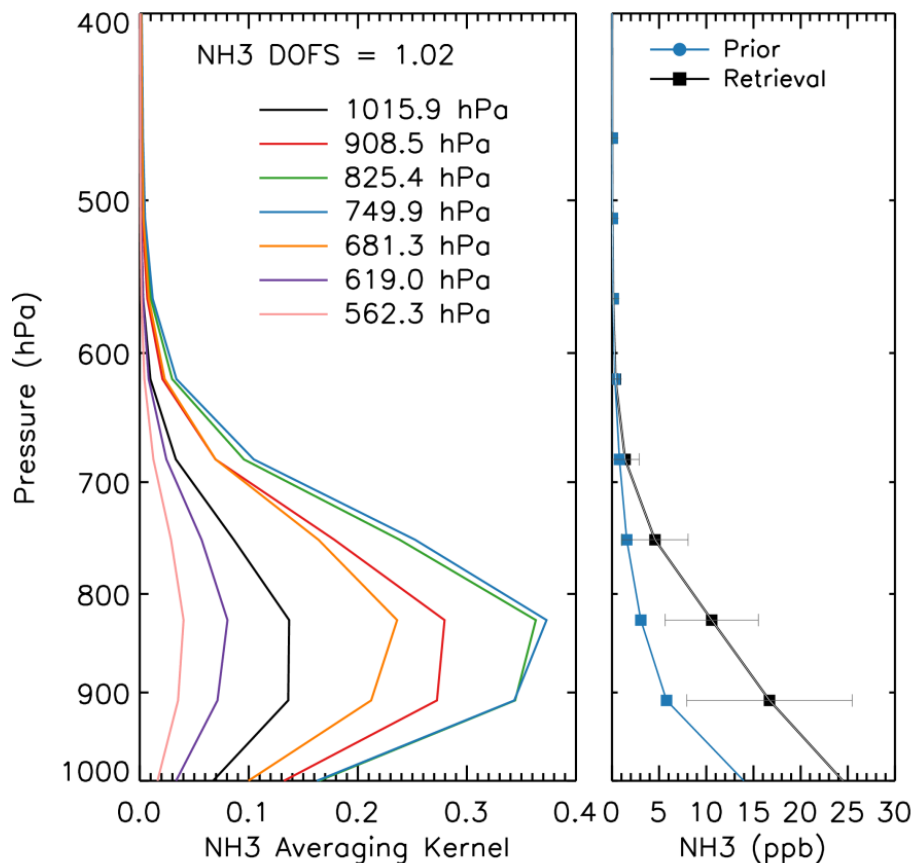


**Figure 5.** Box-and-whiskers plot of the simulated values from Fig. 4 for the peak NH<sub>3</sub> profile values, measurement sensitivity (DOFS), and temperature contrast, all binned as a function of |SNR|. The boxes edges are the 25th and 75th percentile, the line in the box is the median, the diamond is the mean, the whiskers are the 10th and 90th percentiles, and the circles are the outlier values outside the whiskers.

**Cris satellite observations of NH<sub>3</sub>**M. W. Shephard and  
K. E. Cady-Pereira

**Figure 6.** Observed CrIS brightness temperature spectrum over the San Joaquin Valley ( $35.97^{\circ}$  N,  $119.28^{\circ}$  W on the 28 January 2013). Second panel: Brightness temperature residuals (observed minus OSS simulation) with no NH<sub>3</sub> included in the atmospheric profile. Third panel: Brightness temperature residuals after the addition of an NH<sub>3</sub> profile with a mixing ratio of 17.4 ppb at 908 hPa. Fourth panel: Difference between the OSS model runs in the second and fourth panels, showing the spectral signature of NH<sub>3</sub> at the CrIS resolution. The red line in the residual plots highlights the spectral region used in the NH<sub>3</sub> retrievals.

[Title Page](#)[Abstract](#)[Introduction](#)[Conclusions](#)[References](#)[Tables](#)[Figures](#)[|◀](#)[▶|](#)[◀](#)[▶](#)[Back](#)[Close](#)[Full Screen / Esc](#)[Printer-friendly Version](#)[Interactive Discussion](#)

CrIS satellite observations of NH<sub>3</sub>M. W. Shephard and  
K. E. Cady-Pereira

**Figure 7.** Averaging kernel from a CrIS retrieval from a measurement on 28 January 2013 over the San Joaquin Valley in California (left). A priori and retrieved profile with corresponding error bars are plotted in the right panel.

**Figure 8.** The TES averaging kernel and retrieved profile for the TES pixel that corresponds to the CrIS retrieval plotted in Fig. 7.

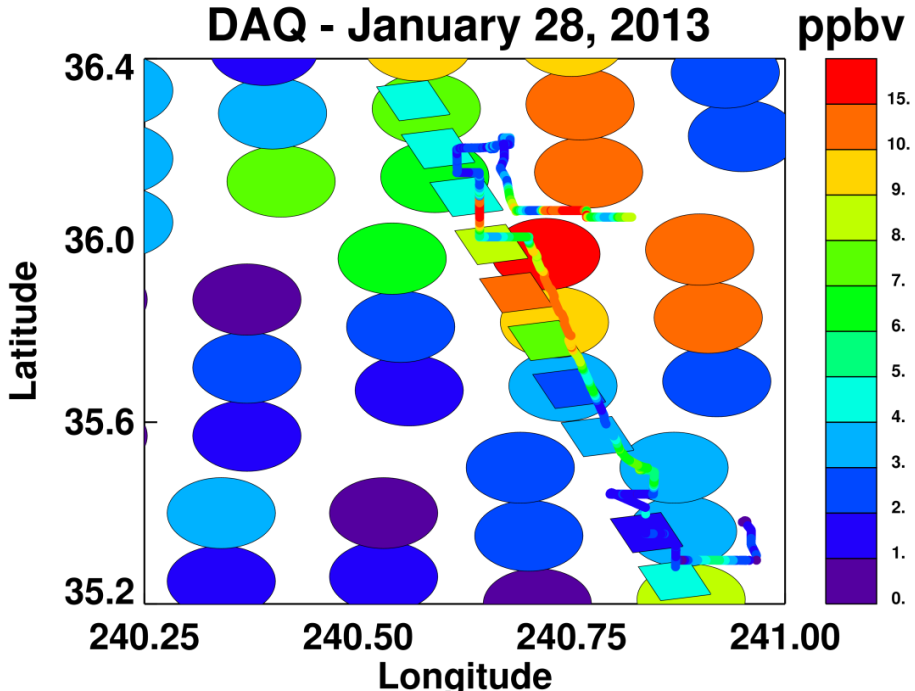


**Figure 9.** Map shows ammonia values from CrIS (large circles), TES (rectangles), and QCL (small circles) on 28 January 2013 during DISCOVER-AQ. The CrIS and TES satellite values are the retrieved results at 900 hPa (peak vertical sensitivity). The QCL values are surface measurements where the values have been scaled by 1/6.

## CrlS satellite observations of NH<sub>3</sub>

M. W. Shephard and  
K. E. Cady-Pereira

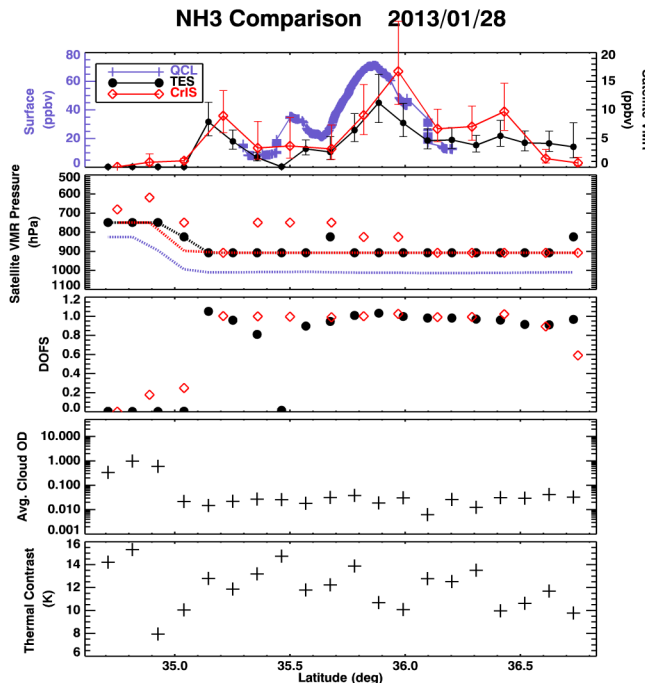


**Figure 10.** NH<sub>3</sub> measurements taken on 28 January 2013 in the San Joaquin Valley in California. The top panel shows surface measurements by the Open Quantum Cascade Laser (QCL) (purple), which are averaged over the coincident TES footprint, and the satellite 900 hPa values from the TES transect observations (black) and the corresponding closest CrlS footprints (red) with total error bars. The symbols in the second panel shows the pressure of peak sensitivity for the satellite observations, with the lines indicating the pressure level of the comparison values shown in the top panel (~ 1 km). The third panel contains the information content from the retrieval in terms of degrees-of-freedom for signal (DOFS). The last two panels show the atmospheric conditions in terms of cloud optical depth (COD) and thermal contrast (surface–atmosphere).